Demonstration of Topological Robustness of Anyonic Braiding Statistics with a Superconducting Quantum Circuit

Chao Song,[1,2] Da Xu,[1] Pengfei Zhang,[1] Jianwen Wang,[2] Qiujiang Guo,[1] Wuxin Liu,[1] Kai Xu,[1] Hui Deng,[2] Keqiang Huang,[4,6] Dongning Zheng,[4,6] Shi-Biao Zheng,[3] H. Wang,[1,2,*] Xiaobo Zhu,[2,5,7,†] Chao-Yang Lu,[2,5,7,‡] and Jian-Wei Pan[2,5,7]

[1]*Department of Physics, Zhejiang University, Hangzhou, Zhejiang 310027, China*
[2]*CAS Center for Excellence and Synergetic Innovation Centre in Quantum Information and Quantum Physics, University of Science and Technology of China, Hefei, Anhui 230026, China*
[3]*Fujian Key Laboratory of Quantum Information and Quantum Optics, College of Physics and Information Engineering, Fuzhou University, Fuzhou, Fujian 350116, China*
[4]*Institute of Physics, Chinese Academy of Sciences, Beijing 100190, China*
[5]*Shanghai Branch, National Laboratory for Physical Sciences at Microscale and Department of Modern Physics, University of Science and Technology of China, Shanghai 201315, China*
[6]*School of Physical Sciences, University of Chinese Academy of Sciences, Beijing 100049, China*
[7]*CAS-Alibaba Quantum Computing Laboratory, Shanghai 201315, China*

(Received 20 March 2018; published 20 July 2018)

Anyons are quasiparticles occurring in two dimensions, whose topological properties are believed to be robust against local perturbations and may hold promise for fault tolerant quantum computing. Here we present an experiment of demonstrating the path independent nature of anyonic braiding statistics with a superconducting quantum circuit, which represents a 7-qubit version of the toric code model. We dynamically create the ground state of the model, achieving a state fidelity of 0.688 ± 0.015 as verified by quantum state tomography. Anyonic excitations and braiding operations are subsequently implemented with single-qubit rotations. The braiding robustness is witnessed by looping an anyonic excitation around another one along two distinct, but topologically equivalent paths: Both reveal the nontrivial π-phase shift, the hallmark of Abelian $1/2$ anyons, with a phase accuracy of $\sim 99\%$ in the Ramsey-type interference measurement.

DOI: 10.1103/PhysRevLett.121.030502

In three-dimensional space, according to the statistical phase obtained during the exchange of two indistinguishable particles, elementary particles are classified into bosons and fermions. Alternatively, theoretically permissible particles called anyons with fractional statistical behavior emerge when it comes to the two-dimensional case [1]. This means that upon two successive exchanges of identical particles, the system wave function acquires a trivial statistical phase for both bosons and fermions, while the statistical phase can take any nontrivial value between 0 and 2π for anyons. Many intriguing properties associated with anyons await further explorations. In particular, the statistical phase associated with the braiding of anyons, i.e., exchange of anyons, is resilient to local fluctuations, based upon which schemes for topological quantum computing and other applications [2–6] have been proposed. Artificially engineered spin lattices with ultracold atoms [7], and multipartite entangled graph states with single photons, nuclear magnetic spins, and superconducting qubits [8–11] have been used as simulation platforms [12] for exploration of the exotic properties of anyons [4,13,14]. However, despite the extensive research effort, there have been few experiments that can demonstrate the topological robustness of anyonic braiding operations [11], which is the key to fault tolerance in topological quantum computing.

One notable proposal to mimic the fractional statistics of anyons is the toric code model, which describes a two-dimensional spin lattice with qubits located on the edges [4]. The Hamiltonian of this model is

$$H = -\sum_v A_v - \sum_f B_f, \tag{1}$$

where $A_v = \prod_{j \in \mathrm{star}(v)} X_j$ for each vertex and $B_f = \prod_{j \in \mathrm{boundary}(f)} Z_j$ for each face, which are also known as stabilizer operators, and X (Z) denotes the standard Pauli operator σ_x (σ_z). The ground state $|\psi_g\rangle$ of this Hamiltonian is the eigenstate with eigenvalue $+1$ for all A_v and B_f. A quasiparticle called the e (m) particle exists on the vertex v_j (face f_j) if A_{v_j} (B_{f_j}) acting on the excited state $|\psi_e\rangle$ ($|\psi_m\rangle$) yields eigenvalue -1. Starting from the ground state, by applying a Z (X) rotation on one of the qubits, a pair of e (m) particles is created on the neighboring vertices (faces), as illustrated in Fig. 1(a). Although both e and m particles by themselves are bosons, the mutual statistics between

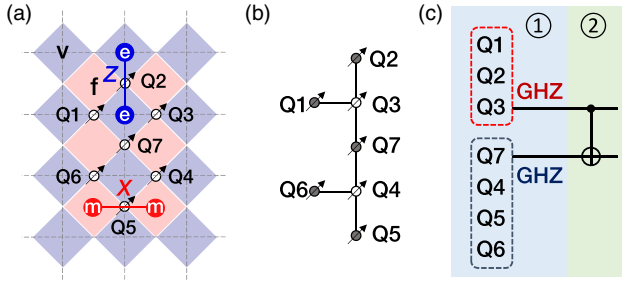

FIG. 1. (a) 7-qubit toric code model. Qubits (balls with arrows), labeled from Q_1 to Q_7, live on the edges of the spin lattice. Two types of quasiparticles, called e and m particles, reside on the vertices (light blue) and the faces (light red), respectively, which can be created by Z and X rotations acting on neighboring qubits once the system is prepared in the ground state $|\psi_g\rangle$ of the toric code Hamiltonian. (b) 7-qubit graph state derived from the layout in (a), which can be obtained by dynamically initializing all qubits in $(|0\rangle + |1\rangle)/\sqrt{2}$ and subsequently applying controlled π-phase (CZ) gates on neighboring qubits connected by lines. This graph state is equivalent to $|\psi_g\rangle$ up to single-qubit Hadamard gates acting on qubits in gray. (c) Sequence diagram for preparing the ground state $|\psi_g\rangle$, which consists of two steps: (i) Create two separated GHZ states; (ii) apply a CNOT gate on Q_3 and Q_7.

them obeys that for Abelian 1/2 anyons [15], which means that a π phase flip occurs if an e (m) particle loops around an m (e) particle. The topological braiding robustness indicates that this π phase flip remains invariant under variations of the braiding path.

Several experiments have used the smallest-scale systems [7–10], and observed a nontrivial π phase flip. However, the path-independent nature of topological braidings has only been explored with a 7-qubit nuclear magnetic resonance simulator [11]. It is known, however, that the liquid nuclear magnetic resonance system cannot prepare pure quantum states and in Ref. [11] the decoherence leads to a relatively large deviation of 0.15π in the phase detection. Here we turn to a solid-state system [16,17], a superconducting circuit with not only more qubits but also much improved qubit coherence as compared with the device in our previous work [8], where the smallest-scale lattice was constructed with four qubits and the braiding loop was unique. In the new device with seven qubits, we can enlarge the lattice size so that two braiding loops are available, which allows us to directly verify the topological braiding robustness. In our experiment, the 7-qubit ground state and anyonic excitations are measured using quantum state tomography (QST), and the path-independent statistical phase due to topological braidings is observed with an accuracy of ~99% via Ramsey-type interference measurement.

The superconducting circuit used in this experiment is composed of ten frequency-tunable transmon qubits symmetrically coupled to a central resonator (R) with a fixed resonant frequency of $\omega_R \approx 5.795$ GHz [18]: Seven of these ten qubits, whose idle frequencies range from 5.21 to 5.64 GHz, are used to prepare the ground state of the 7-qubit toric code model, while the other 3 qubits are tuned to 4.93, 5.03, and 5.70 GHz, respectively, and are left in their ground states throughout the experiment. Noting the seven qubits by Q_j for $j = 1$ to 7, the circuit Hamiltonian is written as

$$\frac{H}{\hbar} = \omega_R a^+ a + \sum_{j=1}^{7} \omega_j |1_j\rangle\langle 1_j| + \sum_{j=1}^{7} g_j(\sigma_j^+ a + \sigma_j^- a^+), \quad (2)$$

where σ_j^+ (σ_j^-) is the raising (lowering) operator of qubit Q_j, a^+ (a) is the creation (annihilation) operator of R, and g_j is the coupling strength between Q_j and R. ω_j is individually tunable. The performance of individual qubits at relevant frequencies, characterized by the energy relaxation time T_1 and the Gaussian dephasing time T_2^*, and the qubit readout metrics are detailed in Supplemental Material [19].

The most challenging part of the experiment is to prepare the ground state of the 7-qubit toric model, $|\psi_g\rangle = (|0000000\rangle + |0001111\rangle + |1110001\rangle + |1111110\rangle)/2$, which is, up to single-qubit Hadamard gates, equivalent to the graph state illustrated in Fig. 1(b) [21]. Instead of using the conventional method with six CZ gates and up to twelve Hadamard gates [15] for the graph state, here we produce $|\psi_g\rangle$ in two steps: (i) Divide the 7 qubits into two clusters with $A = \{1, 2, 3\}$ and $B = \{4, 5, 6, 7\}$, and entangle all qubits in the same cluster to a Greenberger-Horne-Zeilinger (GHZ) state; (ii) apply a CNOT gate to connect the two clusters, as shown in Fig. 1(c).

In step (i), we use two different interaction frequencies for the two qubit clusters to simultaneously mediate the qubit-qubit couplings necessary for generating the two GHZ states [22,23]. We first apply an $X/2$ rotation (the $\pi/2$ rotation around x axis) to each qubit at its idle frequency, where a 15-ns full width at half maximum (FWHM) Gaussian-shape microwave pulse with a full length of 30 ns is used for the $\pi/2$ rotation. The phase of the microwave pulse is calibrated referencing to the frame rotating at the interaction frequency for the corresponding cluster, either ω_A or ω_B [8,18]. Qubits in cluster A are then brought to $\omega_A/2\pi \approx 5.575$ GHz and those in cluster B are brought to $\omega_B/2\pi \approx 5.650$ GHz by applying a square-shaped tuning pulse to each qubit. Qubits in the same cluster become maximally entangled after a duration of $\tau_{A/B} \approx \pi|\Delta_{A/B}|/2g^2$ [22], where $\Delta_{A/B} \equiv \omega_{A/B} - \omega_R$, which gives $\tau_A \approx 140$ ns and $\tau_B \approx 155$ ns. After the required interaction time, all qubits in the same cluster are immediately biased back to their respective idle frequencies for further operations. At this stage, the qubits in each cluster are in an equally weighted superposition of two components, one corresponding to each qubit being polarized along an axis in the $x - y$ plane, and the other one along the opposite direction of the same axis. After applying a second $\pi/2$ rotation around the complementary axis in the $x - y$ plane to each qubit to bring the corresponding axis to the z axis, we obtain the state $|\psi_{\mathrm{GHZ}}\rangle = (\otimes_{j=1}^{3} |0_j\rangle + e^{i\phi_A} \otimes_{j=1}^{3} |1_j\rangle) \otimes (\otimes_{j=4}^{7} |0_j\rangle + e^{i\phi_B} \otimes_{j=4}^{7} |1_j\rangle)/2$, where $\phi_A = 0.612$ and

$\phi_B = -2.396$ are phases due to the particular qubit arrangement that are tracked in software later on; i.e., we implement the zero-duration virtual Z_ϕ rotations on Q_3 and Q_4 to remove ϕ_A and ϕ_B in the following operations and detections [24]. The resulting density matrix of $|\psi_{\mathrm{GHZ}}\rangle$ is characterized by QST [18] with a state fidelity of 0.801 ± 0.008 (see Supplemental Material [19]).

In step (ii), the CNOT gate acting on Q_7 with Q_3 in control is constructed with a two-qubit dressed state gate U plus six single-qubit rotations as shown in Fig. 2(a) [25]. The U gate is 170 ns in length, and is benchmarked by quantum process tomography (QPT) [25,26] with a gate fidelity of 0.950 ± 0.002. All single-qubit gate lengths in Fig. 2(a) are 15 ns FWHM (30 ns full length) Gaussian-shape microwave pulses, and the total length of the CNOT gate is around 260 ns. The CNOT gate is characterized by QPT and has a gate fidelity of 0.925 ± 0.004, with the process matrix χ_{exp} shown in Fig. 2(b).

Since the CNOT gate is optimized separately, in the particular experimental sequence when the CNOT gate is executed, some qubits may acquire unwanted phase drifts due to cross talk. The phase drifts of Q_2, Q_5, and Q_7 are relevant for the experimental accuracy, which are corrected by appending the zero-duration virtual Z_ϕ rotations in all later on operations and detections [24] with the rotation angles ϕ given by -0.150, 0.425, and -0.027, respectively. We then obtain $|\psi_g\rangle$, which is characterized by QST as shown in Fig. 3, with a state fidelity of 0.688 ± 0.015. Once $|\psi_g\rangle$ is prepared, a pair of e particles can be excited by applying a zero-duration virtual Z_π, i.e., Z, rotation on Q_2 as shown in Fig. 1(a) [24], following which the QST characterization of the corresponding excited state $|\psi_e\rangle$ gives a fidelity of 0.682 ± 0.029 (see Supplemental Material [19]).

Compared with QST, correlation measurement offers a more efficient way to distinguish between the ground state $|\psi_g\rangle$ and the excited state $|\psi_e\rangle$. The correlation operator is defined as $P(\gamma) = \otimes_{j=1}^{6} (\cos\gamma Y_j + \sin\gamma X_j)$ [8,27], where γ is the angle between the axis of the polarization to be measured, which is in the $x-y$ plane, and y axis. Here $P(\gamma)$ applies to only six qubits from Q_1 to Q_6, which is sufficient to accurately distinguish between $|\psi_g\rangle$ and $|\psi_e\rangle$ though the visibility of $P(\gamma)$ is reduced after ignoring the outcome of Q_7 (see Supplemental Material [19]). Polarization along the z axis can be experimentally measured for each qubit; Polarization in the $x-y$ plane can be measured after applying a $\pi/2$ rotation to align the polarization with the z axis. With no prior gates the rotation axis would have an angle γ to x axis in the $x-y$ plane; Considering different phases accumulated during the previous virtual Z_ϕ gates for different qubits, the experimental $\pi/2$ rotation axis has an angle of γ for Q_1, $\gamma + 0.150$ for Q_2, $\gamma + 0.612$ for Q_3, $\gamma - 2.396$ for Q_4, $\gamma - 0.425$ for Q_5, and γ for Q_6 with respect to the x axis.

For an arbitrary superposition of $|\psi_g\rangle$ and $|\psi_e\rangle$ in the form of $\cos(\varphi/2)|\psi_g\rangle - i\sin(\varphi/2)|\psi_e\rangle$, the expectation value of $P(\gamma)$ is $\langle P(\gamma)\rangle = [\cos(6\gamma + \pi + \varphi) + \cos\varphi]/2$. Experimentally we repeatedly prepare the target state and perform simultaneous measurements on the six qubits from Q_1 to Q_6, which yield 2^6 occupation probabilities $(P_{000000}, P_{000001}, \ldots, P_{111111})$. The expectation of $P(\gamma)$ can be calculated as

$$\langle P(\gamma)\rangle = \sum_{i_1,i_2,i_3,i_4,i_5,i_6} (-1)^{i_1+i_2+i_3+i_4+i_5+i_6} P_{i_1 i_2 i_3 i_4 i_5 i_6}, \quad (3)$$

where $i_j = 0$ or 1 refers to the $|0\rangle$ or $|1\rangle$ state of qubit Q_j, respectively. The correlation measurement results for $|\psi_g\rangle$, where $\varphi = 0$, and that for $|\psi_e\rangle$, where $\varphi = \pi$, are shown in Figs. 4(a)–4(b), which are fitted according to $\langle P(\gamma)\rangle = b_1\cos(6\gamma + \pi + \varphi) + b_2$, with φ, b_1, and b_2 as the fitting parameters. Here φ is an important parameter which dictates the statistical phase gained during braidings (see next), and we obtain $\varphi_g = (0.000 \pm 0.008)\pi$ for $|\psi_g\rangle$,

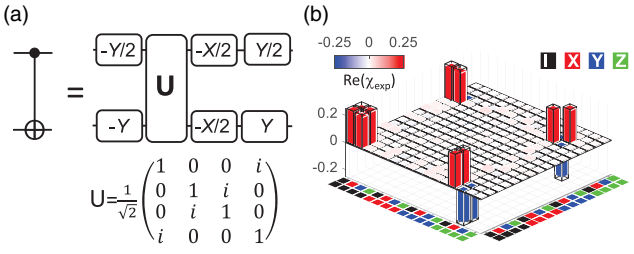

FIG. 2. (a) Sequence diagram for realizing the CNOT gate, which consists of a two-qubit dressed state gate (U, with the matrix form given) and six single-qubit gates. (b) The real part of process matrix χ_{exp} obtained with QPT, showing a process fidelity of $\mathrm{tr}(\chi_{\mathrm{id}}\chi_{\mathrm{exp}}) = 0.925 \pm 0.004$, where χ_{id} is for the ideal CNOT process matrix. All imaginary components are measured to be no higher than 0.029. Color code for the set of the identity and the Pauli operators $\{I, X, Y, Z\}$ is shown in the top right corner, and the first one in the two color squares in the x and y labels indices the control qubit.

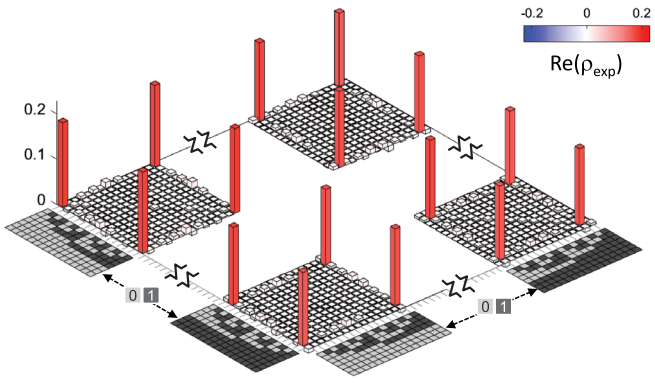

FIG. 3. Partial real part of the experimental density matrix ρ_{exp} for $|\psi_g\rangle$. The state fidelity is $\mathrm{tr}(\rho_{\mathrm{id}}\rho_{\mathrm{exp}}) = 0.688 \pm 0.015$, where ρ_{id} is for the ideal density matrix of $|\psi_g\rangle$. All imaginary components of ρ_{exp} are measured to be no higher than 0.032.

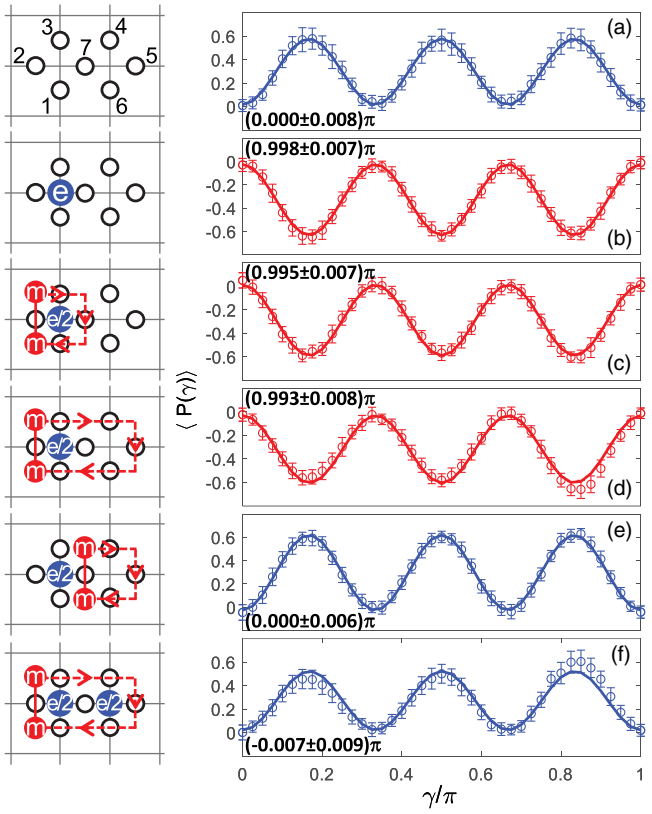

FIG. 4. Observation of the anyonic topological properties with the corresponding lattice realizations shown on the left. (a)–(b) Correlation measurements for the ground state $|\psi_g\rangle$ and the excited state $|\psi_e\rangle$ as illustrated. Solid lines are fits yielding $\varphi_g = (0.000 \pm 0.008)\pi$ in (a) and $\varphi_e = (0.998 \pm 0.007)\pi$ in (b). (c)–(d) Two distinct, but topologically equivalent paths for an m particle to loop around a half-filled e particle vertex (indicated by lines with arrows on the left), with the interference results showing the robustness of anyonic braidings. Solid lines are fits yielding $\varphi_1 = (0.995 \pm 0.007)\pi$ in (c) and $\varphi_2 = (0.993 \pm 0.008)\pi$ in (d). (e) Nonenclosing path which shows no phase flip in the interference. The solid line is a fit yielding $\varphi_3 = (0.000 \pm 0.006)\pi$. (f) Path enclosing two half-filled e particle vertices, with a fit yielding $\varphi_4 = (-0.007 \pm 0.009)\pi$. All fitted phase values of φ agree with theory with accuracies of ~99%.

$\varphi_e = (0.998 \pm 0.007)\pi$ for $|\psi_e\rangle$, both exhibiting the phase accuracies around 99%.

Following the proposal in Ref. [15], we now demonstrate the robustness of anyonic braidings by looping an m particle around an e particle along two different paths. Since the statistical phase acquired is global and unobservable if looping around a fully occupied e particle vertex, here we use the Ramsey-type interference measurement involving a half-filled vertex to detect the phase. Starting from $|\psi_g\rangle$ and with a zero-duration virtual $Z_{\pi/2}$, i.e., $Z/2$, rotation on Q_2 [24], we obtain the superposition $(|\psi_g\rangle - i|\psi_e\rangle)/\sqrt{2}$, so that the two vertices neighboring Q_2 are half-filled with e particles. Two topologically equivalent and nontrivial paths are available for an m particle to loop around the vertex with a half-filled e particle: The first path is illustrated in Fig. 4(c), which is achieved by applying X rotations on Q_1, Q_2, Q_3, and Q_7 successively, with the operator defined as $C_1 = X_7X_3X_2X_1$; the second path is shown in Fig. 4(d), involving the X rotations on six qubits except Q_7 and the operator as $C_2 = X_6X_5X_4X_3X_2X_1$. In practice, since the X operators on different qubits commute with each other, all X rotations are applied simultaneously to minimize the impact of decoherence. After the braidings along the two aforesaid paths, both superpositions become $(|\psi_g\rangle + i|\psi_e\rangle)/\sqrt{2}$ as the same nontrivial π phase is gained on $|\psi_e\rangle$. A subsequent zero-duration virtual $-Z/2$ rotation, acting on Q_2 to annihilate the half-filled e particle generated previously, brings the final state to $|\psi_e\rangle$ instead of $|\psi_g\rangle$. The final state is distinguished with the correlation measurement mentioned above, yielding a fitted phase of $\varphi_1 = (0.995 \pm 0.007)\pi$ for path C_1 and $\varphi_2 = (0.993 \pm 0.008)\pi$ for path C_2. Both paths reveal close statistical phase values with accuracies approaching 99% relative to the π-phase constant, which indicates the topological equivalence of the two paths.

Additional cases are tested. If the m particle loops without surrounding the half-filled e particle vertex or surrounding two half-filled e particle vertices, no statistical phase is expected. Indeed, our correlation measurement with the operator $C_3 = X_7X_6X_5X_4$ yields $\varphi_3 = (0.000 \pm 0.006)\pi$ as shown in Fig. 4(e) and that with C_2 yields $\varphi_4 = (-0.007 \pm 0.009)\pi$ as shown in Fig. 4(f). All these results clearly demonstrate that the statistical phase is only determined by the topological properties of the trajectories.

In conclusion, we have generated the ground state of the 7-qubit toric code model, with a state fidelity of 0.688 ± 0.015 obtained from QST. With this state, the robustness of anyonic topological braiding is demonstrated by looping an m particle around a half-filled e particle vertex along two distinct but topologically equivalent paths, where creation, annihilation, and braiding operations of anyonic excitations are performed with single-qubit rotations. Our experiment not only reveals the exotic properties of anyons, but also may have applications in small-scale topological quantum computing.

This work was supported by the National Natural Science Foundations of China under Grants No. 11434008, No. 11674060, and No. 11574380, the National Basic Research Program of China under Grants No. 2014CB921201, No. 2016YFA0300601, and No. 2017YFA0304300, and the Fundamental Research Funds for the Central Universities of China (Grant No. 2016XZZX002-01), the Chinese Academy of Sciences, and the Anhui Initiative in Quantum Information Technologies. Devices were made at the Nanofabrication Facilities at Institute of Physics in Beijing, University of Science and Technology of China in Hefei, and National Center for Nanoscience and Technology in Beijing.

C. S. and D. X. contributed equally to this work.

*hhwang@zju.edu.cn
†xbzhu16@ustc.edu.cn
‡cylu@ustc.edu.cn

[1] F. Wilczek, Phys. Rev. Lett. **48**, 1144 (1982).
[2] G. K. Brennen and J. K. Pachos, Proc. R. Soc. A **464**, 1 (2008).
[3] C. Nayak, S. H. Simon, A. Stern, M. Freedman, and S. D. Sarma, Rev. Mod. Phys. **80**, 1083 (2008).
[4] A. Y. Kitaev, Ann. Phys. (Amsterdam) **303**, 2 (2003).
[5] R. Raussendorf, J. Harrington, and K. Goyal, New J. Phys. **9**, 199 (2007).
[6] D.-L. Deng, X. P. Li, and S. Das Sarma, Phys. Rev. B **96**, 195145 (2017).
[7] H.-N. Dai, B. Yang, A. Reingruber, H. Sun, X.-F. Xu, Y.-A. Chen, Z.-S. Yuan, and J.-W. Pan, Nat. Phys. **13**, 1195 (2017).
[8] Y.-P. Zhong *et al.*, Phys. Rev. Lett. **117**, 110501 (2016).
[9] C.-Y. Lu, W.-B. Gao, O. Gühne, X.-Q. Zhou, Z.-B. Chen, and J.-W. Pan, Phys. Rev. Lett. **102**, 030502 (2009).
[10] J. K. Pachos, W. Wieczorek, C. Schmid, N. Kiesel, R. Pohlner, and H. Weinfurter, New J. Phys. **11**, 083010 (2009).
[11] A. J. Park, E. McKay, D. Lu, and R. Laflamme, New J. Phys. **18**, 043043 (2016).
[12] I. Georgescu, S. Ashhab, and F. Nori, Rev. Mod. Phys. **86**, 153 (2014).
[13] A. Kitaev, Ann. Phys. (Amsterdam) **321**, 2 (2006).
[14] J.-Q. You, X.-F. Shi, X. Hu, and F. Nori, Phys. Rev. B **81**, 014505 (2010).
[15] Y.-J. Han, R. Raussendorf, and L.-M. Duan, Phys. Rev. Lett. **98**, 150404 (2007).
[16] X. Gu, A. F. Kockumb, A. Miranowicz, Y.-X. Liu, and F. Nori, Phys. Rep. **718–719**, 1 (2017).
[17] P. Roushan *et al.*, Nat. Phys. **13**, 146 (2017).
[18] C. Song *et al.*, Phys. Rev. Lett. **119**, 180511 (2017).
[19] See Supplemental Material at http://link.aps.org/supplemental/10.1103/PhysRevLett.121.030502 for more information on the device performance and the anyonic braiding experiment, which includes Ref. [20].
[20] E. Lucero *et al.*, Phys. Rev. A **82**, 042339 (2010).
[21] M. Hein, J. Eisert, and H. J. Briegel, Phys. Rev. A **69**, 062311 (2004).
[22] S.-B. Zheng, Phys. Rev. Lett. **87**, 230404 (2001).
[23] G. S. Agarwal, R. R. Puri, and R. P. Singh, Phys. Rev. A **56**, 2249 (1997).
[24] D. C. McKay, C. J. Wood, S. Sheldon, J. M. Chow, and J. M. Gambetta, Phys. Rev. A **96**, 022330 (2017).
[25] Q. Guo *et al.*, arXiv:1807.03897.
[26] C. Song *et al.*, Nat. Commun. **8**, 1061 (2017).
[27] T. Monz, P. Schindler, J. T. Barreiro, M. Chwalla, D. Nigg, W. A. Coish, M. Harlander, W. Hänsel, M. Hennrich, and R. Blatt, Phys. Rev. Lett. **106**, 130506 (2011).